

**Max-Planck-Institut
für Mathematik
in den Naturwissenschaften
Leipzig**

**Time-domain Dirichlet-to-Neumann map and its
discretization**

(revised version: February 2012)

by

Lehel Banjai

Preprint no.: 5

2012



Time-domain Dirichlet-to-Neumann map and its discretization

Lehel Banjai

February 20, 2012

Abstract

In this work we address the wave equation in homogeneous, unbounded domains and its numerical solution. In particular we are interested in the effect that the shape of a bounded obstacle has on the quality of some numerical schemes for the computation of the exterior Dirichlet-to-Neumann map. We discretize the Dirichlet-to-Neumann map in time by convolution quadrature and investigate how the correct choice of time-step depends on the highest frequency present in the system, the shape of the scatterer, and the type of convolution quadrature used (linear multistep or Runge-Kutta) and its convergence order.

1 Introduction

Acoustic and electromagnetic scattering problems are naturally posed in infinite domains. An elegant approach that leads to efficient and accurate numerical approximation of such problems is to formulate them as boundary integral equations. For time-harmonic wave propagation, e.g., waves governed by the Helmholtz equation, boundary integral equation methods have become ubiquitous. Boundary integral formulations for general time dependent wave propagation, c.f., wave equation, have been known for as long as their time-harmonic counterparts, nevertheless they have yet to reach the same level of maturity. In this paper we aim to clarify some properties of a class of numerical methods for time-domain boundary integral equations (TDBIE).

A particular class of methods for discretization in time of TDBIE are the so called convolution quadratures (CQ), see [14]. Here an A -stable linear multistep or Runge-Kutta method is used as a basis for a stable quadrature scheme suited to convolution integrals. One of the motivations for using these quadrature rules for TDBIE are their good stability properties. These stability properties, however, come at a price in that low order methods in some cases require exceedingly small time-steps to begin converging. For this reason high-order Runge-Kutta based convolution quadratures have recently gained in popularity [2, 3, 5, 6, 20]. In particular in numerical experiments performed in [3] a big difference could be seen in the performance of low order linear multistep based CQ compared to high-order Runge-Kutta based CQ. This difference proved to be much smaller when wave propagation problems were solved in the exterior of convex obstacles. In the current work we explain these effects, one of the main motivations being the wish to investigate special numerical methods for scattering by one or more convex obstacles [4]. In particular we prove for two special cases (sphere and half-space) and conjecture for general convex obstacles that

$$\| \text{DtN}(s) + s \|_{H^{1/2}(\Gamma) \rightarrow H^{-1/2}} \leq \text{const}$$

holds, where $\text{DtN}(s)$ is the Dirichlet-to-Neumann map for the equation $-\Delta u + s^2 u = 0$ on the exterior of a bounded convex domain Ω with boundary Γ . From this it follows that for convex obstacles both low and high-order methods perform well. For general obstacles higher order methods perform better, in particular convolution quadrature based on Runge-Kutta methods with high (classical) order.

We begin the paper with an introduction to convolution quadrature, then proceed by introducing boundary integral operators, next we investigate the Dirichlet-to-Neumann operator, discuss the dispersion analysis of the numerical scheme, and end with some numerical experiments.

2 Convolution quadrature

Let $K(s)$ be analytic in the half plane $\text{Re } s > 0$ and for some real exponents μ and $\nu \geq 0$ be bounded as

$$|K(s)| \leq C(\sigma) \frac{|s|^\mu}{(\text{Re } s)^\nu} \quad \text{for } \text{Re } s \geq \sigma > 0. \quad (2.1)$$

If $\mu < -1$, the inverse Laplace transform

$$k(t) = (\mathcal{L}^{-1}K)(t) = \frac{1}{2\pi i} \int_{\sigma+i\mathbb{R}} e^{st} K(s) ds, \quad t \geq 1,$$

defines a continuous and exponentially bounded function $k(t)$. In this work, we are interested in computing convolutions of k with a continuous function g ,

$$u(t) = (K(\partial_t)g)(t) := \int_0^t k(t-\tau)g(\tau)d\tau.$$

If $\mu \geq -1$, we define the convolution via the inverse Laplace transform

$$u(t) = (K(\partial_t)g)(t) = \frac{1}{2\pi i} \int_{\sigma+i\mathbb{R}} e^{st} K(s) \mathcal{L}g(s) ds, \quad t \geq 0, \quad (2.2)$$

where if $|\mathcal{L}g(s)| = O(|s|^{-\mu-1-\varepsilon})$, $\varepsilon > 0$, the inverse Laplace transform is well defined. The motivation for the notation $K(\partial_t)g$ comes from identities of the type $K_2(\partial_t)K_1(\partial_t)g = K_2K_1(\partial_t)g$ and $(\partial_t g)(t) = g'(t)$, where for the second example to hold it is necessary that $g(0) = 0$, a condition implied by $|\mathcal{L}g(s)| = O(|s|^{-2-\varepsilon})$.

Another way of writing (2.2) is

$$u(t) = (K(\partial_t)g)(t) = \frac{1}{2\pi i} \int_{\sigma+i\mathbb{R}} K(s)y_g(s)ds, \quad (2.3)$$

where y_g is the solution of the following ODE

$$y' = sy + g, \quad y(0) = 0. \quad (2.4)$$

Convolution quadrature (CQ) of (2.2) is obtained by solving the ODE (2.4) by a linear multistep or Runge-Kutta method and substituting the time-discrete solution back into (2.3), see [12, 13, 5]. Next we give some details regarding the linear multistep and Runge-Kutta based convolution quadrature.

2.1 Linear multistep based CQ

Let $\delta(\zeta)$ be the generating function of an A -stable linear multistep method of order p . This means that $\operatorname{Re} \delta(\zeta) \geq 0$ for $|\zeta| \leq 1$ and that

$$\delta(e^{-z}) = z + O(z^{p+1}). \quad (2.5)$$

For example

$$\delta(\zeta) = 1 - \zeta \text{ for the backward Euler,} \quad \delta(\zeta) = (1 - \zeta) + \frac{1}{2}(1 - \zeta)^2 \text{ for BDF2;}$$

here BDF2 denotes the second order backward difference formula. For time-step $h > 0$, the *convolution weights* $\omega_j^h(K)$ are defined via the expansion

$$K \left(\frac{\delta(\zeta)}{h} \right) = \sum_{j=0}^{\infty} \omega_j^h(K) \zeta^j.$$

Let y_j denote the approximation of $y(t_j)$, $t_j = jh$, obtained by solving (2.4) using the chosen linear multistep method. Denoting the generating function of the solution by $Y(\zeta) = \sum_{j=0}^{\infty} y_j \zeta^j$ and of the data by $G(\zeta) = \sum_{j=0}^{\infty} g_j \zeta^j$, we see that

$$Y(\zeta) = \left(\frac{\delta(\zeta)}{h} - s \right)^{-1} G(\zeta).$$

Substituting this back into (2.3) we obtain

$$U(\zeta) = \frac{1}{2\pi i} \int_{\sigma+i\mathbb{R}} K(s) \left(\frac{\delta(\zeta)}{h} - s \right)^{-1} G(\zeta) ds = K \left(\frac{\delta(\zeta)}{h} \right) G(\zeta),$$

where $U(\zeta) = \sum_{j=0}^{\infty} u_j \zeta^j$ and u_j is an approximation of $u(t_j)$. Comparing the coefficients in the above expression gives

$$u_n = (K(\partial_t^h)g)(t_n) = \sum_{j=0}^n \omega_{n-j}^h(K)g(t_j) = \sum_{j=0}^n \omega_j^h(K)g(t_n - t_j). \quad (2.6)$$

By defining $g(t) \equiv 0$ for $t < 0$, we can define the convolution quadrature approximation $K(\partial_t^h)g$ for all $t \in \mathbb{R}$

$$(K(\partial_t^h)g)(t) = \sum_{j=0}^{\infty} \omega_j^h(K)g(t - t_j). \quad (2.7)$$

A crucial property of CQ is that the composition rule $K_2(\partial_t^h)K_1(\partial_t^h)g = K_2K_1(\partial_t)g$ still holds. A further important remark is that the Laplace transform of the convolution quadrature is easily computed:

$$(\mathcal{L}K(\partial_t^h)g)(s) = \sum_{j=0}^{\infty} \omega_j^h(K)e^{-sjh}(\mathcal{L}g)(s) = K \left(\frac{\delta(e^{-sh})}{h} \right) (\mathcal{L}g)(s). \quad (2.8)$$

The Laplace transform of the exact convolution is by definition, see (2.2), given by $K(s)\mathcal{L}g(s)$. Therefore convolution quadrature is obtained by replacing $K(s)$ with its approximation $K\left(\frac{\delta(e^{-sh})}{h}\right)$. From the properties of $K(s)$ and $\delta(\zeta)$ we can deduce, see [14], that

$$K\left(\frac{\delta(e^{-sh})}{h}\right) = K(s) + s^{p+\mu+1}O(h^p). \quad (2.9)$$

Remark 2.1. From (2.9) we see that if the highest frequency present in the system is ω_{\max} , i.e., $|\mathcal{L}g(s)|$ is negligible for $|s| > \omega_{\max}$ we expect that for a good relative accuracy the time-step needs to be chosen as

$$h \propto \omega_{\max}^{-(p+1)/p}.$$

We see that the higher the order p the closer is this choice to the sampling requirement $h \propto \omega_{\max}^{-1}$. Unfortunately A -stable linear multistep methods are restricted to orders $p \leq 2$. For this reason we will consider Runge-Kutta based CQ as well. Of crucial importance for our discussion will be the fact that even though the estimate (2.9) is optimal for a general $K(s)$ satisfying (2.1), for the special case $K(s) = s$ it is not. In fact from (2.5) we directly obtain that

$$\frac{\delta(e^{-sh})}{h} = s + s^{p+1}O(h^p),$$

instead of the remainder term being $s^{p+2}O(h^p)$ as (2.9) would suggest.

2.2 Runge-Kutta based CQ

An m -stage Runge-Kutta discretization of (2.4) is given by

$$\begin{aligned} Y_{ni} &= y_n + sh \sum_{j=1}^m a_{ij} Y_{nj} + h \sum_{j=1}^m a_{ij} g(t_n + c_j h), \quad i = 1, 2, \dots, m, \\ y_{n+1} &= y_n + sh \sum_{j=1}^m b_j Y_{nj} + h \sum_{j=1}^m b_j g(t_n + c_j h), \end{aligned}$$

where $h > 0$ is the time step, $t_n = nh$, and the internal stages Y_{ni} and grid values y_n are approximations to $y(t_n + c_i h)$ and $y(t_n)$, respectively. We will make use of the notation

$$A = (a_{ij})_{i,j=1}^m, \quad b = (b_1, b_2, \dots, b_m)^T, \quad \mathbb{1} = (1, 1, \dots, 1)^T$$

and

$$R(z) = 1 + zb^T(I - zA)^{-1}\mathbb{1}$$

where the latter is the stability function of the Runge-Kutta method. In the following $p \geq 1$ will denote the (classical) order of the Runge-Kutta method and $q \leq p$ its stage order.

As in [6] we require that the Runge-Kutta method is A -stable, i.e., that $I - zA$ is non-singular for $\operatorname{Re} z \leq 0$ and that $|R(z)| \leq 1$ for $\operatorname{Re} z \leq 0$. Further we assume that $|R(iy)| < 1$ for real $y \neq 0$, $R(\infty) = 0$, and that the coefficient matrix A is invertible. Note that from $R(\infty) = 0$ follows that $b^T A^{-1}\mathbb{1} = 1$.

The convolution weights for the Runge-Kutta based CQ are given by the expansion

$$K\left(\frac{\Delta(\zeta)}{h}\right) = \sum_{j=0}^{\infty} W_j^h(K)\zeta^j,$$

where

$$\Delta(\zeta) = \left(A + \frac{\zeta}{1-\zeta}\mathbb{1}b^T\right)^{-1} = A^{-1} - \zeta A^{-1}\mathbb{1}b^T A^{-1}.$$

Note that in contrast to multistep based CQ, the weights here are matrix valued. The convolution quadrature approximation of (2.2) is given by

$$u^h(t_n) = u_n := b^T A^{-1}K\left(\underline{\partial}_t^h\right)g(t_n),$$

where

$$K\left(\underline{\partial}_t^h\right)g(t) = \sum_{j=0}^{\infty} W_j^h(K)(g(t - t_j + c_j h))_{\ell=1}^m.$$

The composition rule holds in the form $K_2(\underline{\partial}_t^h)K_1(\underline{\partial}_t^h)g = K_2K_1(\underline{\partial}_t^h)g$ and the Laplace transform of $u^h(t)$ is again easily computed

$$(\mathcal{L}u^h)(s) = b^T A^{-1}K\left(\frac{\Delta(e^{-sh})}{h}\right)e^{csh}e^{-sh},$$

where $e^c = (e^{c_1}, e^{c_2}, \dots, e^{c_m})^T$. One of the main results proved in [6] is that

$$b^T A^{-1}K\left(\frac{\Delta(e^{-sh})}{h}\right)e^{csh}e^{-sh} = K(s) + s^{p+\mu+1}O(h^p) + s^{q+1}O(h^{q+1-\mu+\nu}), \quad (2.10)$$

compare this with (2.9). We will also need the following result, which should be compared with (2.5).

Lemma 2.2. *For $\operatorname{Re} z > 0$ it holds*

$$b^T A^{-1} \Delta(e^{-z}) e^{cz} e^{-z} = z + O(z^{q+1}). \quad (2.11)$$

Proof. For the proof of this result we will make use of the fact that $b^T A^{-1} \mathbb{1} = 1$ and of equations (8) and (9) in [6, Lemma 2] which we restate here:

$$z b^T e^{cz} = e^z - 1 + O(z^{p+1}) \quad (2.12)$$

and

$$z A e^{cz} = e^{cz} - \mathbb{1} + O(z^{q+1}). \quad (2.13)$$

From this it follows that

$$A^{-1} e^{cz} = A^{-1} \mathbb{1} + z e^{cz} + O(z^{q+1})$$

and

$$b^T A^{-1} e^{cz} = e^z + O(z^{q+1}).$$

Hence

$$b^T A^{-1} \Delta(e^{-z}) e^{cz} e^{-z} = b^T A^{-1} (A^{-1} - e^{-z} A^{-1} \mathbb{1} b^T A^{-1}) e^{cz} e^{-z} = z + O(z^{q+1}).$$

□

Remark 2.3. *As in the linear multistep case, see Remark 2.1, we discuss here the correct choice of h . From (2.10) we see that if the highest frequency present in the system is ω_{\max} , we expect that the relative error is of the form*

$$\omega_{\max} (\omega_{\max} h)^p + h^\nu (\omega_{\max} h)^{q+1-\mu},$$

hence for a good relative accuracy and large ω_{\max} we need to choose

$$h \propto \omega_{\max}^{-(p+1)/p}.$$

Here it is important that the classical order p is involved and not the significantly lower stage order q , see also the discussion on dispersion and dissipation in [7].

Again, it is of crucial importance for our discussion to notice the difference in the estimates (2.10) and (2.11) in the special case $K(s) = s$.

3 Time-domain boundary integral equations

Let $\Omega^- \subset \mathbb{R}^d$, $d = 2$ or $d = 3$, be a bounded Lipschitz domain with boundary $\Gamma = \partial\Omega^-$ and let $\Omega^+ = \mathbb{R}^d \setminus \overline{\Omega^-}$ be its complement. We consider the wave equation

$$u'' - \Delta u = 0, \quad \text{in } \Omega^+ \times [0, T] \quad (3.1a)$$

$$u(x, t) = g(x, t), \quad \text{on } \Gamma \times [0, T] \quad (3.1b)$$

$$u(x, 0) = u'(x, 0) = 0, \quad x \in \Omega^+, \quad (3.1c)$$

where we assume $g(\cdot, t) \in H^{1/2}(\Gamma)$ and require $u(\cdot, t) \in H^1(\Omega^+)$.

Remark 3.1. *The above problem should be understood as scattering by a sound soft obstacle, where an incident wave $u^{inc}(x, t)$ with the trace $u^{inc}|_{\Gamma} = -g$ is scattered by the obstacle Ω^- . The total wave u^{tot} is zero on the boundary and the scattered wave is given by the difference $u = u^{tot} - u^{inc}$.*

In order to introduce boundary integral operators we will require some notation. The exterior normal vector to the boundary Γ will be denoted by n , the exterior trace by γ^+ , the interior by γ^- , and the exterior and interior normal derivative by ∂_n^+ and ∂_n^- respectively.

To construct the time domain integral representation of the scattering problem, we will need the fundamental solution for the d'Alembert operator. In two and three dimensions these are given by:

$$k(x, t) = \begin{cases} \frac{H(t - |x|)}{2\pi\sqrt{t^2 - |x|^2}} & \text{in 2D,} \\ \frac{\delta(t - |x|)}{4\pi|x|} & \text{in 3D.} \end{cases} \quad (3.2)$$

The single layer potential has $k(\cdot, \cdot)$ as its kernel

$$S(\partial_t)\varphi(x, t) := \int_0^t \int_{\Gamma} k(x - y, t - \tau)\varphi(y, \tau)d\Gamma_y d\tau, \quad (x, t) \in \mathbb{R}^d \setminus \Gamma \times (0, \infty) \quad (3.3)$$

and the double layer potential has the normal derivative of $k(\cdot, \cdot)$ as its kernel

$$D(\partial_t)\varphi(x, t) := \int_0^t \int_{\Gamma} \partial_{n_y} k(x - y, t - \tau)\varphi(y, \tau)d\Gamma_y d\tau, \quad (x, t) \in \mathbb{R}^d \setminus \Gamma \times (0, \infty) \quad (3.4)$$

The single layer potential is continuous across the boundary Γ and we can define its trace, the so-called single layer operator, with the same formula

$$V(\partial_t)\varphi(x, t) := \int_0^t \int_{\Gamma} k(x-y, t-\tau)\varphi(y, \tau)d\Gamma_y d\tau, \quad (x, t) \in \mathbb{R}^d \setminus \Gamma \times (0, \infty). \quad (3.5)$$

The double layer, does however have a jump

$$\gamma^- D(\partial_t)\varphi - \gamma^+ D(\partial_t)\varphi = -\varphi. \quad (3.6)$$

Consequently, we define the corresponding boundary operator by

$$K(\partial_t)\varphi(x, t) := \frac{1}{2}(\gamma^+ + \gamma^-)D(\partial_t)\varphi. \quad (3.7)$$

From the last two equations it follows that

$$\gamma^\pm D(\partial_t)\varphi = \pm \frac{1}{2}\varphi + K(\partial_t)\varphi.$$

The solution of (3.1) can be written in terms of the above operators applied to its Cauchy data:

$$u(x, t) = -S(\partial_t)\partial_n^+ u + D(\partial_t)\gamma^+ u = -S(\partial_t)\partial_n^+ u + D(\partial_t)g, \quad (x, t) \in \Omega^+ \times (0, \infty).$$

Taking the exterior trace we obtain the boundary integral equation for the unknown Cauchy data $\varphi = \partial_n^+ u$:

$$V(\partial_t)\varphi = \left(-\frac{1}{2}I + K(\partial_t)\right)g. \quad (3.8)$$

In order to state the existence and uniqueness of the solution of the above equation we will make use of the following space. For $m \in \mathbb{N}_0$ and $k \in \mathbb{R}$ let

$$W^{m,1}(\mathbb{R}; H^k(\Gamma)) := \{g : \partial_t^m g \in L^1(\mathbb{R})\}, \quad (3.9)$$

where \mathcal{F} denotes the Fourier transform in the variable t and

$$W_0^{m,1}((0, T); H^k(\Gamma)) := \{g|_{(0, T)} : g \in W^{m,1}(\mathbb{R}; H^k(\Gamma)) \text{ with } g(\cdot, t) \equiv 0, t \in (-\infty, 0)\}. \quad (3.10)$$

For any $g \in W_0^{4,1}((0, T); H^{1/2}(\Gamma))$ there exists a unique $\varphi \in C((0, T); H^{-1/2}(\Gamma))$ that solves (3.8), see [14, Lemma 2.2]. The mapping $g \mapsto \varphi$ which solves (3.8) is called the exterior Dirichlet-to-Neumann operator and will be denoted by

$$\text{DtN}^+(\partial_t) : W_0^{4,1}((0, T); H^{1/2}(\Gamma)) \rightarrow C((0, T); H^{-1/2}(\Gamma)). \quad (3.11)$$

We will also make use of the Laplace domain counterparts of the above operators. These have the fundamental solution of the Helmholtz operator $-\Delta \cdot + s^2 \cdot$ as the kernel:

$$K(x, s) = \begin{cases} \frac{1}{4} K_0(s|x|) & \text{in 2D,} \\ \frac{e^{-s|x|}}{4\pi|x|} & \text{in 3D.} \end{cases} \quad (3.12)$$

The single and double layer potentials are defined analogously:

$$\begin{aligned} S(s)\varphi(x) &:= \int_{\Gamma} K(x-y, s)\varphi(y)d\Gamma_y, & x \in \mathbb{R}^d \setminus \Gamma, \\ D(s)\varphi(x) &:= \int_{\Gamma} \partial_{n_y} K(x-y, s)\varphi(y)d\Gamma_y, & x \in \mathbb{R}^d \setminus \Gamma, \\ V(s)\varphi(x) &:= \int_{\Gamma} K(x-y, s)\varphi(y)d\Gamma_y, & x \in \Gamma, \\ K(s)\varphi(x) &:= \frac{1}{2}(\gamma^+ + \gamma^-)D(s)\varphi, \\ \text{DtN}^+(s) &:= V^{-1}(s) \left(-\frac{1}{2}I + K(s) \right), \end{aligned}$$

where it is throughout assumed that $\text{Re } s > 0$. The mapping properties of these operator are as follows

$$\begin{aligned} V(s) &: H^{-1/2}(\Gamma) \rightarrow H^{1/2}(\Gamma), \\ K(s) &: H^{1/2}(\Gamma) \rightarrow H^{1/2}(\Gamma), \\ \text{DtN}(s) &: H^{1/2}(\Gamma) \rightarrow H^{-1/2}(\Gamma). \end{aligned}$$

The main aim of this paper is the investigation of convolution quadrature of $\text{DtN}(\partial_t)$. With this in mind we investigate the Dirichlet-to-Neumann map in more detail in the next section.

4 The Dirichlet-to-Neumann map

As has already been noted in [3], the behaviour of the convolution quadrature approximation of the boundary integral equations can depend strongly on whether the scattering obstacle is convex or not. Further, in [4] we specifically consider the computation of scattering by one or more convex obstacles, where results stated here are of great importance. For this reason, we begin our investigation with convex obstacles.

4.1 The Dirichlet-to-Neumann operator for convex domains

4.1.1 The case of the unit sphere: $\Gamma = \mathbb{S}^2$

Let Y_ℓ^m denote the spherical harmonics which build an orthonormal basis of $L^2(\mathbb{S}^2)$, see [16]. We will use these to construct Sobolev spaces on \mathbb{S}^2 in the usual way, see [15, Chapter X, §6]. Further, in [10, 16] we find that Y_ℓ^m are eigenfunctions of boundary integral operators for the Helmholtz equations,

$$\begin{aligned} V(s)Y_\ell^m &= \lambda_\ell(s)Y_\ell^m, & K(s)Y_\ell^m &= \mu_\ell(s)Y_\ell^m, \\ \text{DtN}(s)Y_\ell^m &= \nu_\ell(s)Y_\ell^m, \end{aligned}$$

with eigenvalues

$$\begin{aligned} \lambda_\ell(s) &= -sh_\ell(is)j_\ell(is), & \mu_\ell(s) &= -1/2 - is^2h_\ell(is)j'_\ell(is), \\ \nu_\ell(s) &= \frac{-1 - is^2h_\ell(is)j'_\ell(is)}{-sh_\ell(is)j_\ell(is)}, \end{aligned}$$

where j_ℓ and h_ℓ are spherical Bessel functions of first and second kind, respectively. We are particularly interested in investigating the eigenfunctions of the Dirichlet-to-Neumann operator.

Proposition 4.1. *For $s \in \mathbb{C}$ and $\ell = 0, 1, \dots$ it holds*

$$\nu_\ell(s) = -s - \ell - 1 + s \frac{\theta'_\ell(s)}{\theta_\ell(s)}$$

where

$$\theta_\ell(s) = \sum_{k=0}^{\ell} (\ell, k) s^{\ell-k}, \quad (\ell, k) = \frac{(\ell+k)!}{2^k k! (\ell-k)!}.$$

Proof. The proof can be found in [18, Chapter 9, Section 9]. About the properties of the reverse Bessel polynomials $\theta_\ell(z)$ one can read in [9, Section 4.10]. \square

Corollary 4.2. *There exists a constant $C > 0$ such that for $\operatorname{Re} s \geq 0$ and $\ell \in \mathbb{N}_0$*

$$|\nu_\ell(s) + s| \leq C(\ell + 1).$$

From this it follows that

$$\|\operatorname{DtN}(s) + s\|_{H^{1/2}(\mathbb{S}^2) \rightarrow H^{-1/2}(\mathbb{S}^2)} \leq \text{const}, \quad \text{for } \operatorname{Re} s \geq 0. \quad (4.1)$$

Proof. Let $\lambda_{\ell,j}$, $j = 1, 2, \dots, \ell$ be the zeros of $\theta_\ell(s)$. From [9, Section 4.10] we know that the zeros are simple and belong to the annulus

$$\lambda_{\ell,j} \in \left\{ z \in \mathbb{C} : \frac{\ell + 1}{2} \leq |z| < \frac{2\ell + 4/3}{2} \right\}. \quad (4.2)$$

Further, since the zeros of $\theta_\ell(s)$ are also the scattering poles, we know that, see [11], there exists $\sigma > 0$ such that $\operatorname{Re} \lambda_{\ell,j} \leq -\sigma$ for all ℓ and j .

It follows that

$$s \frac{\theta'_\ell(s)}{\theta_\ell(s)} = \sum_{j=1}^{\ell} \frac{s}{s - \lambda_{\ell,j}} = \sum_{j=1}^{\ell} \frac{\lambda_{\ell,j}}{s - \lambda_{\ell,j}} + \ell.$$

If $|s| \leq (\ell + 1)/4$ or $|s| > 2\ell + 4/3$ then from the above expressions and (4.2) the required result is easy to deduce.

The result for the case $|s| \sim \ell$ follows directly from the asymptotic estimates [1, (9.3.7)–(9.3.20)], which completes the proof. \square

Remark 4.3. *The situation is similar in two dimensions. Here the eigenfunctions are $e^{i\ell\theta}$ and*

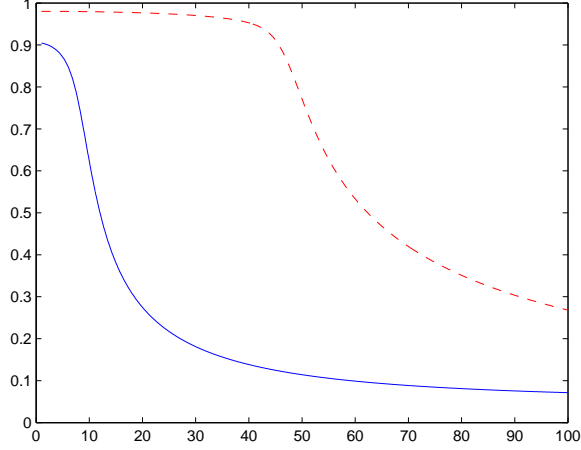
$$\operatorname{DtN}(s)e^{i\ell\theta} = \frac{-1 + sI'_\ell(s)K_\ell(s)}{I_\ell(s)K_\ell(s)} = s \frac{K'_\ell(s)}{K_\ell(s)},$$

where in the last step we have used the expression for the Wronskian given in [1, (9.6.15)]. Unlike in 3D, the operator above is not a simple rational function. Nevertheless, the following numerical experiment indicates that the bound $|\nu_\ell(s) + s| \leq C(1 + \ell)$ holds here as well.

```

DtN = @(s,1) 1-s.*besselk(1+1,s,1)./besselk(1,s,1);
s = 1+1i*linspace(1,100,1000);
plot(imag(s),abs(DtN(s,10)+s)/10); hold on;
plot(imag(s),abs(DtN(s,50)+s)/50,'r--');

```



4.1.2 The half-space and the general convex case

Theorem 4.4. Let $\mathbb{R}_+^d = \{x = (x_1, \dots, x_d) \in \mathbb{R}^d : x_d > 0\}$, $\Gamma_+ = \partial\mathbb{R}_+^d = \{x \in \mathbb{R}^d : x_d = 0\}$, $d = 2$ or $d = 3$. Given $\psi \in H^{1/2}(\Gamma_+)$ with finite support and $s \in \mathbb{C}$ such that $\text{Re } s > 0$, let $v \in H^1(\mathbb{R}_+^d)$ be the unique solution of

$$\begin{aligned} -\Delta u + s^2 u &= 0, & \text{in } \mathbb{R}_+^d, \\ u &= \psi, & \text{on } \Gamma_+. \end{aligned}$$

Then

$$\|\partial_n u|_{\Gamma_+} + s\psi\|_{H^{-1/2}(\Gamma_+)} \leq C\|\psi\|_{H^{1/2}(\Gamma_+)},$$

where C is a constant independent of s .

Proof. To solve the problem, we compute the Fourier transform in the first $d - 1$ coordinates:

$$\hat{u}(\xi', x_d) = \int_{\mathbb{R}^2} e^{i\xi' \cdot x'} u(x) dx',$$

where $x' = (x_1, \dots, x_{d-1})$ and $\xi' = (\xi_1, \dots, \xi_{d-1})$. Then \hat{u} should solve

$$\partial_{x_d}^2 \hat{u} = (|\xi'|^2 + s^2)\hat{u}, \quad \hat{u}|_{\Gamma_+} = \hat{\psi}.$$

The solution is given by $\hat{u} = \hat{\psi}(\xi')e^{-x_d\sqrt{|\xi'|^2+s^2}}$, with the usual branch-cut along the negative real axis, and hence

$$\partial_n \hat{u}|_{\Gamma_+} = \frac{d}{dx_d} \hat{u}|_{\Gamma_+} = -\sqrt{|\xi'|^2 + s^2} \hat{\psi}.$$

Notice that with $z = s/|\xi'|$ it holds

$$|s - \sqrt{|\xi'|^2 + s^2}| = |s - s\sqrt{1 + (|\xi'|/s)^2}| = |\xi'| |z - z\sqrt{1 + z^{-2}}|.$$

The function $f(z) = z - z\sqrt{1 + z^{-2}}$ is analytic for $\operatorname{Re} z > 0$ and bounded by 1 on $\operatorname{Re} z = 0$ and $\lim_{\substack{\operatorname{Re} z > 0 \\ |z| \rightarrow \infty}} f(z) = 0$, hence

$$|s - \sqrt{|\xi'|^2 + s^2}| \leq |\xi'| \leq (1 + |\xi'|^2)^{1/2}. \quad (4.3)$$

Next, note that the norm $\|\psi\|_{H^k(\Gamma_+)}$ is equivalent to $\left(\int_{\mathbb{R}^{d-1}} (1 + |\xi'|^2)^k |\hat{\psi}|^2\right)^{1/2}$. Hence to estimate $\|\partial_n u|_{\Gamma_+} + s\psi\|_{H^{-1/2}(\Gamma_+)}$ we compute

$$\begin{aligned} \int_{\mathbb{R}^{d-1}} (1 + |\xi'|^2)^{-1/2} |\partial_n \hat{u}|_{\Gamma_+} + s\hat{\psi}|^2 d\xi' &= \int_{\mathbb{R}^{d-1}} (1 + |\xi'|^2)^{-1/2} |s - \sqrt{|\xi'|^2 + s^2}|^2 |\hat{\psi}|^2 d\xi' \\ &\leq \int_{\mathbb{R}^{d-1}} (1 + |\xi'|^2)^{1/2} |\hat{\psi}|^2 d\xi' \leq \text{const} \|\psi\|_{H^{1/2}(\Gamma)}^2. \end{aligned}$$

With this the proof is finished. \square

Remark 4.5. *The above result shows that the Dirichlet-to-Neumann map on the half space has the same property (4.1) as it has for the spherical scatterer. We conjecture that the same is true for a general smooth and convex scatterer. This conjecture is supported by the fact that for a smooth and convex domain there are no diffracted or reflected waves that can destroy the local nature of the DtN operator and hence affect the type of analysis done for the half-space.*

An interesting case is a non-smooth convex domain, e.g., a square. Here the corners become sources of diffracted waves. This brings some non-local effects that may change the behaviour of the Dirichlet-to-Neumann map, but these non-local effects may be small.

4.2 The Dirichlet-to-Neumann operator for a non-convex obstacle

For a general obstacle we do not expect $\| \text{DtN}^+(s)\psi + s\psi \|_{H^{-1/2}(\Gamma)} \leq C\|\psi\|_{H^{1/2}(\Gamma)}$ to hold. An indication for this is given by looking at the interior DtN operator acting on the sphere:

$$\text{DtN}^-(s)Y_\ell^m = V^{-1}(s) \left(\frac{1}{2} + K(s) \right) Y_\ell^m = \nu_\ell^- Y_\ell^m,$$

where

$$\nu_\ell^- = \frac{1/2 + \mu_\ell}{\lambda_\ell} = \frac{isj'_\ell(is)}{j_\ell(is)}.$$

In particular for $\ell = 0$ we get, see [1, (10.1.11)],

$$\nu_0^- = -1 + is \tan(is).$$

The tangent term oscillates along lines parallel to the imaginary axis and no leading term as simple as s can be taken out in contrast to the convex case.

This is a simple example, but it does illustrate that for a scatterer with a cavity in which the incident wave can be trapped, we do not expect such simple result as in the convex case to hold.

5 Dissipation, dispersion, and scattering poles

A common method to investigate qualitative properties of a numerical discretization of a differential equation, is to investigate its dissipation and dispersion properties. For CQ discretization of TDBIE, this has been done in [17] for linear multistep methods and in [7] for Runge-Kutta methods. These works have however not explained the difference that can occur between convex and non-convex domains. For sake of completeness, we give a few comments regarding this type of analysis.

As explained in [14] for linear multistep based CQ, solving the CQ discretized TDBIE is equivalent to solving the original PDE, discretized in time by the underlying linear multistep method. In detail, this means that if $\varphi^h = \text{DtN}(\partial_t^h)g$, then

$$u^h := -S(\partial_t^h)\varphi^h + D(\partial_t^h)g$$

is the unique solution of the time discretized wave equation

$$-\Delta u + (\partial_t^h)^2 u = 0, \quad \text{in } \Omega^+ \times [0, T], \quad (5.1a)$$

$$\gamma^+ u = g, \quad \text{on } \Gamma \times [0, T] \quad (5.1b)$$

$$u(x, 0) = u'(x, 0) = 0, \quad \text{in } \Omega^+. \quad (5.1c)$$

Similar statement can be made for the Runge-Kutta based CQ, see [3, 7].

Dissipation and dispersion analysis constitutes the investigation of plane wave solutions $u(x) = e^{i\zeta \cdot x - i\omega t}$ of (3.1a) and semi-discrete plane-wave solutions $u_n^h(x) = e^{i\zeta \cdot x - i\omega^h t_n}$ of (5.1a). The exact dispersion relation is $|\zeta|^2 = \omega^2$, whereas the discrete dispersion relation is given by

$$|\zeta|^2 = \left(\frac{\delta(e^{-i\omega^h h})}{ih} \right)^2.$$

For example for the backward Euler method this gives

$$\omega^h = \pm|\zeta| + \frac{i}{2}h|\zeta|^2 \mp \frac{1}{3}h^2|\zeta|^3 + \dots$$

This shows that there is both dispersion and dissipation in the discrete scheme, in contrast to the exact wave equation. In particular for the first order method the plane wave solution has size $\sim e^{-\frac{1}{2}h|\zeta|^2}$. Therefore to get a physically correct solution we require $h \ll |\zeta|^{-2}$ which is a much stronger condition than the sampling condition of $h \ll |\zeta|^{-1}$. This is equivalent to the conclusions of the previous sections for non-convex domains, but much more pessimistic for convex scatterers. In order to understand the difference between the two cases also with regards to the dispersion analysis, it helps to ask ourselves whether plane wave solutions develop at all in scattering problem.

Plane wave solutions of (3.1) cannot occur for all times $t \geq 0$ because of the initial condition, but perhaps can develop at later times. Let us, without loss of generality, by for example employing a partition of unity on g , assume that for some $t_0 > 0$, $g(x, t) \equiv 0$ for $t > t_0$. Solutions of the type $u(x, t) = e^{-i\omega t} \hat{u}(x)$, for $t > t_0$, can occur if there exists a non-zero \hat{u} which solves

$$\begin{aligned} -\Delta \hat{u} - \omega^2 \hat{u} &= 0, & \text{in } \Omega^+, \\ \gamma^+ \hat{u} &= 0, & \text{on } \Gamma, \\ \hat{u} &\sim C \frac{e^{i\omega r}}{r}, & \text{for } r = |x| \rightarrow \infty, \end{aligned} \quad (5.2)$$

where the last condition means that u is an outgoing solution.

We know, see [11, 18], that non-zero solutions of (5.2) occur only for a certain discrete set of frequencies called *scattering poles* which satisfy $\text{Im } \omega < 0$. In this case however, $u(x, t)$ has infinite energy, which disqualifies it as a solution of (3.1). Nevertheless, see Epilogue in [11], we know that for trapping domains the scattering poles can be arbitrarily close to the real axis. Therefore in this case solutions that are nearly plane waves can occur and the above dissipation and dispersion analysis is valid and indeed points to possible difficulties in using low order methods. On the other hand it is known, see again [11], that for convex or star-shaped domains the scattering poles are well separated from the real axis, so that such effects might have less influence. The effects of possible non-normality of the DtN operator are also of importance, in which case it is the pseudo-spectrum of the operators rather than the spectrum that is important; see [19] for a recent book on pseudospectra and [8] for a recent investigate of the normality of boundary integral operators.

In conclusion, this type of analysis also suggests that the numerical results may be better for convex domains than for a general non-convex domain, though it doesn't give such quantitative results for the correct choice of time-step as the analysis in Section 4. Further, the discussion of scattering poles suggests that the numerical results may also behave well for non-convex but star-shaped domains. This we investigate in the section on numerical experiments.

6 Numerical experiments

6.1 A space independent example

We start with a very simple experiment, that nevertheless very nicely illustrates the analysis from Section 4. Let $K_1(s) = s + e^{-s}$ and $K_2(s) = s + se^{-s}$. We will compute the error in computation of $K_j(\partial_t)g$ with BDF2 and 3-stage Radau IIA methods for the data

$$g(t) = \begin{cases} \sin^3(\omega t) & t \geq 0, \\ 0 & t < 0 \end{cases}$$

and various values of ω . Note that

$$K_1(\partial_t)g = g'(t) + g(t - 1), \quad K_2(\partial_t)g = g'(t) + g'(t - 1).$$

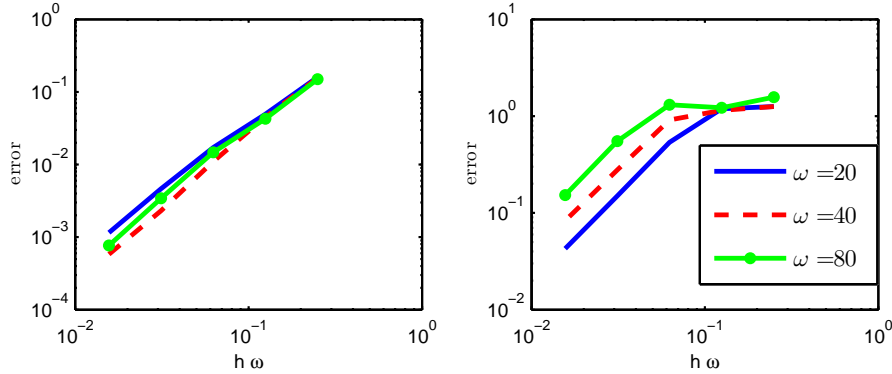


Figure 1: Convergence of the BDF2 based convolution quadrature, on the left for $K_1(s) = s + e^{-s}$ and on the right for $K_2(s) = s + se^{-s}$.

Both functions satisfy (2.1) with $\mu = 1$ and $\nu = 0$, but discussion in remarks 2.1 and 2.3 suggests that the error

$$\text{error} = \max_{0 \leq i \leq N} \omega^{-1} |K_j(\partial_t)g(t_i) - K_j(\partial_t^h)g(t_i)|, \quad t_i = ih, T = Nh = 2,$$

with $h = \text{const} \omega^{-1}$ will be constant in the case $j = 1$ and increasing in the case $j = 2$. The results shown in figures 1 and 2 support this conclusion. This indeed mimics the difference between computing the exterior with the computation of the interior Dirichlet-to-Neumann map for the unit sphere. For more experiments on the unit sphere see [3]. Let us here just note the obvious fact that the error on the interval $[0, 1]$ in the two cases would be identical, differences would only be visible for $t > 1$ once the first “reflection” has occurred.

6.2 Examples in \mathbb{R}^2

We consider the scattering of an incident wave by three two-dimensional domains:

- An ellipse defined by

$$\Gamma = \left\{ \left(\frac{1}{3} \cos(\theta) + \frac{1}{6} \cos(\theta) + \frac{1}{2}, \frac{1}{3} \sin(\theta) - \frac{1}{6} \sin(\theta) + \frac{1}{2} \right) ; \theta \in [0, 2\pi) \right\}.$$

- Square with corners at $(0, 0)$, $(1, 0)$, $(1, 1)$, and $(0, 1)$.

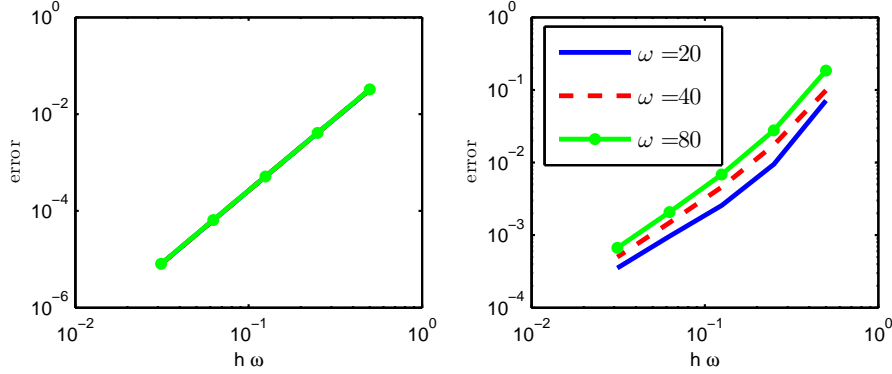


Figure 2: Convergence of the 3-stage Radau IIA based convolution quadrature, on the left for $K_1(s) = s + e^{-s}$ and on the right for $K_2(s) = s + se^{-s}$. The three curves on the left cannot be distinguished at this scale.

- L-shaped domain, the corners of which are given by $(1/2, 0)$, $(1, 0)$, $(1, 1)$, $(0, 1)$, $(0, 1/2)$, and $(1/2, 1/2)$.

The incident wave is a plane wave travelling in the direction α :

$$u^{\text{inc}}(t, x) = f\left(\frac{1}{\varrho}(t - x \cdot \alpha + A)\right), \quad f(t) = e^{-t^2}.$$

The scattered wave u solves the wave equation (3.1) with the right-hand side $g = -u^{\text{inc}}|_{\Gamma}$ in the time interval $[0, T]$ with $T = 5$. Note that the incident wave does not vanish at the origin, however our choice of constants A and ϱ will ensure that its value at the origin is very small.

We formulate the problems as a boundary integral equation, discretize in time by a BDF2 based convolution quadrature, and in space by a Galerkin boundary element method. A fine spatial discretization is fixed and the time discretization is computed for $h = 1/40, 1/80, 1/160, 1/320$. The computed normal derivative is denoted by φ^h . Since the exact solution is not available, the relative error for time-step $h = 1/40, 1/80, 1/160$ is approximated by

$$\text{error} = \frac{\max_{t_j \in [0, T]} \|\varphi^h(t_j, \cdot) - \varphi^{h/2}(t_j, \cdot)\|_{H^{-1/2}(\Gamma)}}{\max_{t_j \in [0, T]} \|\varphi^{h/2}(t_j, \cdot)\|_{H^{-1/2}(\Gamma)}},$$

where the $H^{-1/2}(\Gamma)$ is computed by using the definition of the norm via the single-layer potential

$$\|\varphi\|_{H^{-1/2}(\Gamma)}^2 = (V(\sigma)\varphi, \varphi)_{L^2(\Gamma)},$$

ϱ	h	ellipse	square	L-shape
3/4	1/40	0.015	0.019	0.022
3/8	1/80	0.018	0.023	0.035
3/16	1/160	0.018	0.023	0.042

Table 1: Error for the ellipse, square, and L-shaped domain.

with some $\sigma = 1$ and approximating this value by discretizing $V(\sigma)$ with the same Galerking method.

For the ellipse and the L-shaped domain we send an incident wave in the direction $\alpha = \frac{1}{\sqrt{2}}(1, 1)$ and choose $A = \sqrt{2}/4 - 5/2$; note that this ensures that multiple reflections occur for the L-shape. For the square the incident wave travels in the direction $\alpha = \frac{1}{\sqrt{2}}(-1, -1)$ and we set $A = -\sqrt{2}/4 - 5/2$.

Note that since the Fourier transform of $f(t/\varrho)$ is given by

$$\int_{-\infty}^{\infty} e^{-i\omega t} f(t/\varrho) dt = \varrho \sqrt{\pi} e^{-\frac{(\varrho\omega)^2}{4}},$$

the largest frequencies excited are proportional to ϱ^{-1} . Hence the optimal choice of h would be $h \propto \varrho$. The behaviour of the error is given in Table 1 for the three different scatterers and various ϱ .

As the theory predicted, the choice $h \propto \varrho$ is sufficient to conserve constant relative error in the case of a smooth convex scatterer. The same seems to hold true for the square scatterer, meaning that the refracted waves do not have a strong influence on convergence. As soon as multiple reflections occur in the case of the L-shaped domain, i.e., a non-convex but star-shaped domain, the error does increase with decreasing ϱ .

7 Concluding remarks

We have shown that detailed knowledge of the DtN map is needed in order to understand the behaviour of the convolution quadrature approximation in the case of an incident wave with a high-frequency content. In particular we have argued that

$$\| \text{DtN}(s) + s \|_{H^{1/2}(\Gamma) \rightarrow H^{-1/2}} \leq \text{const}$$

holds for smooth convex obstacles and that it implies good qualitative properties of both low order linear multistep and high-order Runge-Kutta methods.

The numerical experiments here and in [3] support this. Whether the obstacle is smooth or not does not seem to influence the results. Non-convexity, even for non-trapping domains, however does make the effectiveness of low-order methods deteriorate with increasing frequency content. Therefore for all but convex obstacle one is advised to use high-order Runge-Kutta methods.

References

- [1] M. Abramowitz and I. A. Stegun, editors. *Handbook of mathematical functions with formulas, graphs, and mathematical tables*. Dover Publications Inc., New York, 1992.
- [2] J. Ballani, L. Banjai, S. Sauter, and A. Veit. Numerical solution of exterior Maxwell problems by Galerkin BEM and Runge-Kutta convolution quadrature. *submitted*, 2011.
- [3] L. Banjai. Multistep and multistage convolution quadrature for the wave equation: Algorithms and experiments. *SIAM J. Sci. Comput.*, 32(5):2964–2994, 2010.
- [4] L. Banjai and F. Ecevit. Time-domain scattering by one or more convex obstacles. *work in progress*, 2012.
- [5] L. Banjai and C. Lubich. An error analysis of Runge-Kutta convolution quadrature. *BIT*, 51(3):483–496, 2011.
- [6] L. Banjai, C. Lubich, and J. M. Melenk. Runge-Kutta convolution quadrature for operators arising in wave propagation. *Numer. Math.*, 119(1):1–20, 2011.
- [7] L. Banjai and M. Schanz. Wave propagation problems treated with convolution quadrature and BEM. *Accepted as chapter in: "Fast Boundary Element Methods in Engineering and Industrial Applications"*, 2010.
- [8] T. Betcke, J. Phillips, and E. Spence. Spectral decompositions and non-normality of boundary integral operators in acoustic scattering. *submitted*, 2012.
- [9] M. E. H. Ismail. *Classical and quantum orthogonal polynomials in one variable*, volume 98 of *Encyclopedia of Mathematics and its Applications*.

Cambridge University Press, Cambridge, 2005. With two chapters by Walter Van Assche, With a foreword by Richard A. Askey.

- [10] R. Kress and W. T. Spassov. On the condition number of boundary integral operators for the exterior Dirichlet problem for the Helmholtz equation. *Numer. Math.*, 42(1):77–95, 1983.
- [11] P. D. Lax and R. S. Phillips. *Scattering theory*, volume 26 of *Pure and Applied Mathematics*. Academic Press Inc., Boston, MA, second edition, 1989. With appendices by Cathleen S. Morawetz and Georg Schmidt.
- [12] C. Lubich. Convolution quadrature and discretized operational calculus I. *Numer. Math.*, 52:129–145, 1988.
- [13] C. Lubich. Convolution quadrature and discretized operational calculus II. *Numer. Math.*, 52:413–425, 1988.
- [14] C. Lubich. On the multistep time discretization of linear initial-boundary value problems and their boundary integral equations. *Numer. Math.*, 67:365–389, 1994.
- [15] S. G. Mikhlin and S. Prössdorf. *Singular integral operators*. Springer-Verlag, Berlin, 1986.
- [16] J.-C. Nédélec. *Acoustic and electromagnetic equations*, volume 144 of *Applied Mathematical Sciences*. Springer-Verlag, New York, 2001.
- [17] X. W. Q. Chen, P. Monk and D. Weile. Analysis of convolution quadrature applied to the time-domain electric field integral equation. *Commun. Comput. Phys.*, 11:383–399, 2012.
- [18] M. E. Taylor. *Partial differential equations. II*, volume 116 of *Applied Mathematical Sciences*. Springer-Verlag, New York, 1996. Qualitative studies of linear equations.
- [19] L. N. Trefethen and M. Embree. *Spectra and pseudospectra*. Princeton University Press, Princeton, NJ, 2005. The behavior of nonnormal matrices and operators.
- [20] X. Wang and D. S. Weile. Implicit Runge-Kutta methods for the discretization of time domain integral equations. *IEEE Trans. Antennas and Propagation*, 59(12):4651–4663, 2011.